*Published in the Journal of Reinforced Plastics and Composites, vol 19, no. 1, 2000, pp 15-33.*
*Guo and Cox (1998)*

# An Interface Model for the Mechanical Interaction between FRP Bars and Concrete

JUN GUO AND JAMES V. COX
*Department of Civil Engineering*
*Johns Hopkins University*
*Baltimore, Maryland 21218*

**ABSTRACT:** Modeling the behavior of concrete reinforced with fiber-reinforced plastic (FRP) bars requires models for the constitutive behavior of concrete and FRP and a model for their interaction. This study focuses upon modeling the mechanical interaction between FRP bars and concrete. The interaction (commonly called *bond*) can be dominated by mechanical effects when the bars have a significant surface structure. A phenomenological bond model that was originally developed and applied to steel bars is applied to the bond of FRP bars. The model provides a macroscopic characterization of the bond behavior within the mathematical framework of elastoplasticity theory. While the bond model has been applied to both steel and FRP bars, the failure mechanisms can be quite different, thus application of the model to the bond of FRP bars merits critical evaluation. Among the important differences is the potential failure of the surface structure of the bar. The phenomenological model is defined to characterize the structural behavior associated with surface structure failure, but it will not predict the state of damage in the FRP bar. A unique aspect of the formulation is the potential to predict longitudinal cracking in the adjacent concrete. Calibration and validation results are presented to highlight the potential strengths and weaknesses of the model. The model gives surprisingly accurate predictions of bond strength for four independent experimental studies. It does not predict the variation of bond strength with embedment length observed in one set of tests, but other results from the same study suggest the apparent variation could be due to experimental scatter. Additional experimental data for calibration and validation of the model using a common FRP bar are needed to further evaluate the application of the model, but the results from this initial study indicate the model could potentially be used to evaluate the behavior of structural components reinforced with FRP bars.

**Key words:** surface structure, interface, FRP bar, concrete, mechanical interaction, elastoplasticity, bond

## 1. INTRODUCTION

The desperate state of much of the nation's infrastructure and potential advantages of composite materials (*e.g.*, improved life cycle costs) has led to increased interest in applying composite materials to civil engineering structures. One application is the use of fiber-reinforced plastic (FRP) reinforcing bars for concrete, as an alternative to steel reinforcing bars. The resistance of FRP bars to environmental elements makes their application attractive for many applications, *e.g.*, waterfront structures, highway systems subjected to winter salting, and containment structures for corrosive materials. Other favorable properties of FRP reinforcing bars include: high strength/weight ratio, electromagnetic neutrality, and ease of handling. There are also many issues for FRP bars that merit additional investigation, among them are: durability (*e.g.*, the potential of chemical degradation of glass fibers within an alkaline environment), behavior of FRP bars under sustained loads, and the brittle behavior of FRP bars. There have been numerous tests on the behavior of FRP-reinforced concrete (see *e.g.*, Nanni [1993]), but the analysis of FRP-reinforced concrete has received less attention.

Modeling the behavior of FRP-reinforced concrete requires models for the constitutive behavior of concrete and FRP and a model for their interaction. This study focuses upon modeling the interaction (commonly called *bond*) between FRP bars having a significant surface structure and concrete; for this case, bond behavior is dominated by the mechanical interaction between the surface structure of the bar and the adjacent concrete matrix. As for any composite material, the interaction between the reinforcement and matrix is important toward understanding the failure of the composite.

In recent years, researchers have conducted many experimental studies on the bond between FRP bars and concrete (see *e.g.*, Faza and GangaRao [1990], Saadatmanesh and Ehsani [1991], Larralde and Silva-Rodriguez [1993], Nanni [1993], ACI [1994], Larralde *et al.* [1994], Malvar [1994, 1995], Schmechpeper and Goodspeed [1994], Taerwe [1995], Belarbi *et al.* [1996], Benmokrane *et al.* [1996], Ehsani *et al.* [1997], Tepfers *et al.* [1997], Larralde *et al.* [1998], and Tepfers[1998]). Many of the studies were conducted to help determine design criteria for the bond of FRP bars. Researchers have also sought to identify the nature of the bond failure (*e.g.*, failure of the concrete versus failure of the surface structure of the FRP bar) and to compare the bond strength and stiffness of steel and FRP bars (see *e.g.*, Larralde and Silva-Rodriguez [1993], Malvar [1994], and Tepfers *et al.* [1997]).

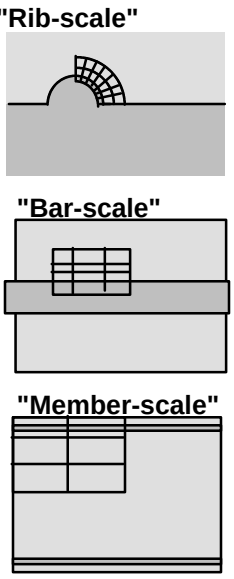


***Figure 1**. Scales of bond analysis.*

Bond has been numerically modeled and characterized at several scales. Figure 1 depicts three scales of bond modeling with names that reflect the scale of spatial discretization (Cox and Herrmann [1992, 1998]); however, not all bond models fit neatly into these three categories. At a relatively large scale – the *member-scale*, each reinforcing element is treated as a one-dimensional bar element and bond is characterized by a bond stress-slip relationship. The member scale can allow realistic structural problems to be addressed, but this scale also has limitations; *e.g.*, it is too coarse to predict some behaviors such as the propagation of longitudinal cracks[1] to a free surface (which essentially eliminates bond strength). At a much smaller scale – the *rib-scale*, the bar and its surface structure are often explicitly modeled (*e.g.*, the complex shape of the bar's surface may be discretized with finite elements). Rib-scale analyses are very important toward understanding aspects of the underlying mechanics of bond, but generally the simplifying assumptions made limit the models to qualitative evaluations. Furthermore, this scale is too fine for most practical analyses. A scale of compromise – the *bar-scale* – treats the bar and concrete as continua and models the interaction between them without explicitly modeling the surface structure of the bar. This type of model has a phenomenological nature, but potentially it can be used to model the behavior of structural components while including important failure mechanisms such as longitudinal cracking of the concrete adjacent to the bars.

For steel bars, there have been several bond models proposed at each of the above scales, but only a few models have been proposed for FRP bars. As for steel bars, the first bond models for FRP bars have addressed the member scale; see *e.g.*, the models of Faoro (1992), Malvar (1994), Alunno *et al.* (1995), and Cosenza *et al.* (1995, 1997). Faoro (1992), and Alunno *et al.* (1995) applied the model of Eligehausen *et al.* (1983) which was originally developed for steel bars. The model of Cosenza *et al.* (1995, 1997) was also based upon the model of Eligehausen *et al.* (1983) but the ascending portion of the bond stress-slip relationship was modified. These models relate average bond stress to slip and were derived from curve fits to a single data set. Thus member-scale models generally have two important limitations: (1) they will only predict bond response in structures having a stress history similar to the original specimen, and (2) they can not produce longitudinal cracking in the adjacent concrete. A few rib-scale models have also been proposed. Boothby *et al.*[74](1995) present a rib-scale analysis of a bond specimen having

[1] Consider a cylindrical coordinate system with the z-axis coincident with the axis of the bar. Ideal longitudinal cracks would occur in a θ-coordinate plane.

an FRP bar with a single rib. The FRP is modeled with an elastoplastic model using a modified Hill criterion, and the concrete is modeled with an unspecified elastoplastic model. Yonezawa *et al.*[7] (1993) also presented a simple parameter study (based upon rib-scale analyses) to determine the effects of rib geometry on the stresses within the concrete and FRP; however, their analyses were apparently based on the assumption of linear elastic material behavior.

This study addresses the characterization of bond behavior between FRP bars and concrete at the *bar-scale*. A bond model that was originally developed for steel bars is applied to the bond of FRP bars. The model provides a macroscopic characterization of the bond behavior within the mathematical framework of elastoplasticity theory. While the application of the mathematical model is herein extended to FRP bars, the underlying mechanics can be very different. The surface structure geometry and mechanical properties of FRP bars differ significantly from those of steel bars. As such, the effects of the mechanical interaction can produce different failure modes; *e.g.*, one mode of failure that can occur with FRP bars (but not for steel bars) is a mode II fracture of the bar's surface structure. Since the initial application of the bar-scale model to FRP bars will not incorporate physical parameters related to constitutive behavior of FRP, we anticipate that the model will have to be recalibrated for bars having significantly different surface structures.

The next section of this paper presents an overview of the elastoplastic bond model of Cox and Herrmann (1992, 1998, 1999; Cox [1994]) with the calibration parameters for a particular FRP bar. The calibration is obtained via simplified analyses of the experimental results of Malvar (1994, 1995) for his "type d" bars. Section three presents the calibration and validation results. The validation results are obtained by using the model to simulate the behavior of other bond specimens reported in the literature. The last section presents conclusions highlighting the strengths and weaknesses of the modeling approach.

## 2. ELASTOPLASTIC BOND MODEL

There are several underlying assumptions associated with bar-scale models (see *e.g.*, Cox and Herrmann [1998]); a common assumption is that the interaction can be characterized by an interface model. For some bars this is obviously an idealization, since the region around the bar that is affected by the mechanical interaction (the *bond zone*) can have a significant thickness. Another assumption is that the interface traction can be homogenized to yield a continuous traction distribution. The generalized stresses (**Q**) can then be defined as the tangent and normal components of the interface traction, $\tau$ and $\sigma$ respectively. $\tau$ is referred to as the *bond stress*, and $-\sigma$ will be referred to as the *confinement stress*. ($\sigma$ is positive in tension.) The generalized strains (**q**) are defined as the tangent ($\delta_t$) and normal ($\delta_n$) displacements of the concrete surface measured relative to the bar surface and nondimensionalized by the bar diameter ($D_b$); *i.e.*, $\mathbf{q}^T = (\delta_t/D_b,\ \delta_n/D_b)$. For monotonic loading, the evolution of the yield surface is characterized by a single measure of the internal state, the bond zone "damage" which is defined as

$$d = \min\left(\frac{\delta_t^p}{s_r},\ 1\right) \tag{1}$$

where $\delta_t^p$ is the plastic slip and $s_r$ is a characteristic length of the surface structure (*e.g.*, the length of a unit surface element for a periodic surface structure). The terminology "damage" indicates that $d$ is a measure of the physical damage at the rib-scale, but it does not imply that the bar-scale model is based upon the concepts of damage mechanics.

The yield criterion is of the form $f(\tau, \sigma, d) = 0$ with

$$f(\tau,\sigma,d) = \frac{|\tau|}{f_t} - C(d)\left\{W(d)\left[1-\exp\left(-\alpha_e\left[\hat{\sigma}(d)-\frac{\sigma}{f_t}\right]\right)\right] + M(1-W(d))\left|\hat{\sigma}(d)-\frac{\sigma}{f_t}\right|^{\alpha_p}\right\} \tag{2}$$

where: $f_t$ is the tensile strength of concrete; $C$ is the isotropic hardening/softening function; $\hat{\sigma}$ is the kinematic softening function; $W$ is the weighting function; and $M$, $\alpha_e$ and $\alpha_p$ are model

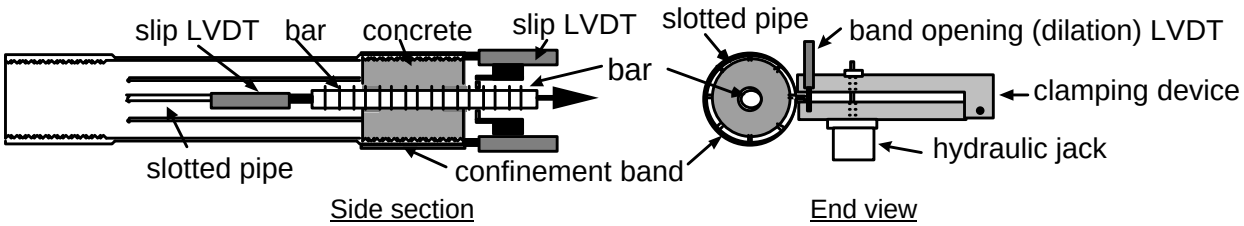


***Figure 2**. Schematic of Malvar test specimen.*

parameters. For the current calibration, $W = 0$, $M = 1$ and $\alpha_p = 0.75$. That is, the form of the model was simplified for this application to only include the "power function" of the two component functions of $\sigma$.

The calibration used in this study is based upon the test results of Malvar (1994,1995) for a "type d" bar – a 19 mm diameter bar. We anticipate that the model will only reproduce experimental results for specimens with similar concrete strengths and bars having a very similar surface structure. The series of experimental tests conducted by Malvar are particularly useful for formulating and calibrating phenomenological models, since they provide data at different stress states. Figure 2 shows a schematic of the test specimen proposed by Malvar (1994). This specimen is a small concrete cylinder with a diameter of 3 in. (76.2 mm), a length of 4 in. (101.6 mm), and a bonded length of 2.625 in. (67 mm). The specimen is cast within a slotted pipe that is later enclosed in a circumferential band. This band is used to apply uniform normal tractions to the outer surface of the specimen and to measure the change in circumference. The slotted pipe apparatus is loaded under displacement control in a common testing frame. A hydraulic clamp (with an adjustable relief valve) is used to apply constant confining pressure. LVDTs are used to measure the longitudinal displacement at both ends of the specimen and to measure the change in circumference. Malvar subjected the bars to normal tractions at five different levels of compression; the intensity of the normal traction was defined as the average radial traction at the bar that would occur if the concrete did not carry hoop stress (500, 1500, 1500, 3500, and 4500 psi; *i.e.*, 3.45, 10.3, 17.2, 24.1, and 31.0 MPa). His tests included a "pre-load" to split the concrete specimen prior to performing the bond tests, so the initial extent of damage in the bar surface structure and concrete is unknown.

Figure 3 shows the graphs of $C$ and $\hat{\sigma}$ that were obtained by examining the test results of Malvar (1994). These two functions completely characterize the evolution of the yield surface, the dominant feature of which is the softening behavior. Isotropic softening represents a progressive failure of the bond zone, while the kinematic softening is physically associated with the change in contact forces between the surface structure of the bar and the adjacent concrete. Figure 4 shows the yield surface at three stages: (1) the initial surface ($d$=0), (2) at the state of maximum isotropic hardening, and (3) at the purely frictional state (*i.e.*, $d$=1 – a totally damaged bond zone).

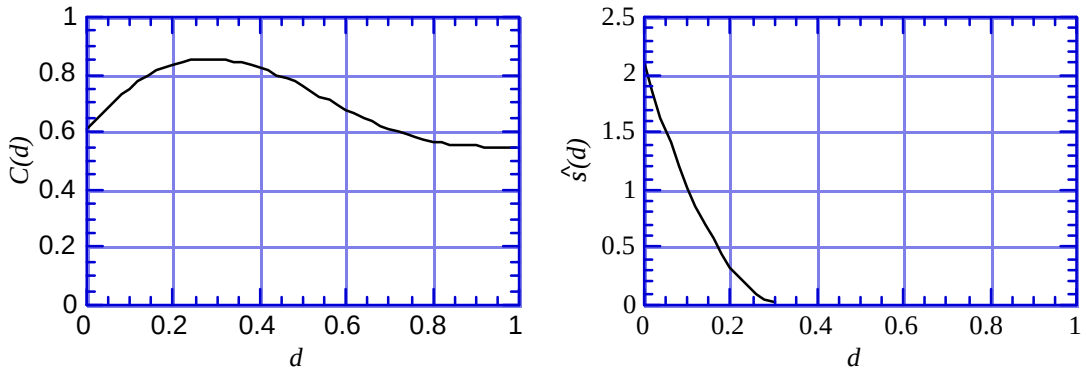


***Figure 3**. Isotropic hardening/softening function C(d) and the kinematic softening function $\hat{\sigma}(d)$.*

The strains are additively decomposed into elastic ($\mathbf{q}^e$) and plastic ($\mathbf{q}^p$) components. The relationship between stresses ($\mathbf{Q}$) and elastic strains ($\mathbf{q}^e$) is assumed to have the linear form

$$\mathbf{Q} = \mathbf{D}^e \mathbf{q}^e \tag{3}$$

The elastic moduli are defined as

$$\mathbf{D}^e = \begin{bmatrix} E_c / k_0 & 0 \\ 0 & E_c / (k_1 + k_2 q_2^p) \end{bmatrix} \tag{4}$$

where $E_c$ is Young's modulus of the concrete, and $k_0$, $k_1$, and $k_2$ are model parameters. $k_0$ is obtained by calibration, prescribing the parameter so that model accurately reproduces the initial elastic bond stress-slip behavior. When $k_2$ is nonzero, the model has elastoplastic coupling. The physical argument for this mathematical form is based upon the change in the actual interface traction distribution and the damage of constituent materials (Cox [1996]). The effect of the interface traction distribution can be obtained in closed form for an idealized case (see *e.g.*, Cox and Yu [1998]). For the calibration used here, these parameters are taken to have the following values: $k_0 = 10$, $k_1 = 0.034$, and $k_2 = 27$.

The kinematics of the wedging action of the bar's surface structure is accounted for in the bar-scale model through the flow rule, which initially produces radial dilation of the interface. The following form was adopted to simplify the flow rule description

$$\dot{\mathbf{q}}^p = \dot{\lambda} \begin{Bmatrix} \mathrm{sgn}(\tau) \\ g(\sigma, d) \end{Bmatrix} \tag{5}$$

where $\dot{\lambda}$ denotes the consistency parameter. To obtain an approximation for $g$, limited data presenting radial dilation versus slip (Malvar [1994]) were analyzed. We assumed that: (1) $g$ is only dependent upon $-\sigma$ and $d$, (2) the $-\sigma$ value reported by Malvar (1994) is the normal stress at the bar surface, and (3) the radial elastic contraction due to the applied confinement stress is not significant. The resulting model approximation of $g$ is shown in Figure 5. As defined by equation (5), $g$ represents the rate of plastic radial dilation with respect to plastic slip; thus, the area under each curve is proportional to the maximum radial dilation. An important behavior for the model to capture is the decrease in radial dilation with an increase in the confinement stress. Unlike member-scale models, the bar-scale model actively contributes to the stress state near the bar through the radial dilation and thus can produce longitudinal cracking in the concrete matrix.

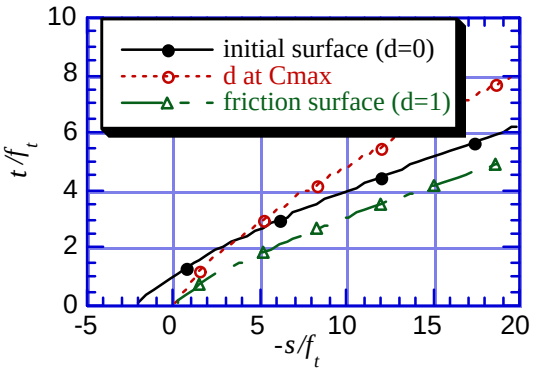


***Figure 4***. *Yielding surfaces.*

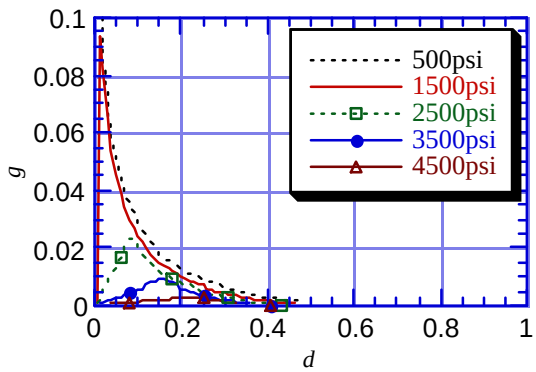


***Figure 5***. *Flow rule.*

## 3. CALIBRATION AND VALIDATION

In this section, we present selected calibration and validation results to establish some of the capabilities and limitations of the bond model. Preliminary validation results that incorporated less accurate models of bond specimens were previously presented (Guo and Cox [1998]). The calibration is based upon the tests of Malvar (1994) as discussed in the previous section. The validation tests compare model results with the experimental pull-out results of Brown and Bartholomew (1993), Larralde and Silva-Rodriguez (1993), Larralde *et al.* (1994), and Tepfers *et al.* (1997). Comparisons of the model results with the experimental results of Brown and Bartholomew (1993), Larralde and Silva-Rodriguez (1993), and Larralde *et al.* (1994) are limited to peak bond strength, while comparisons of bond stress versus slip are presented for the data of Malvar (1994) and Tepfers *et al.* (1997). The particular experimental studies were selected because the surface structures of their bars resembled that of the "type d" bars used by Malvar, and the concrete strengths were also close to that of Malvar. The surfaces have a helical indentation that is produced by a bundle of glass fibers that is wound around the bar during the pultrusion process (see Figure 6). Figure 7 shows schematics (at a common scale) of all the experimental specimens considered in this study.

***Figure 6**. FRP bar with a helical surface structure.*

An inherent difficulty in characterizing bond behavior is that it can not be experimentally isolated; it is integrally tied to the bond specimen, since it is a structural response. Thus, to

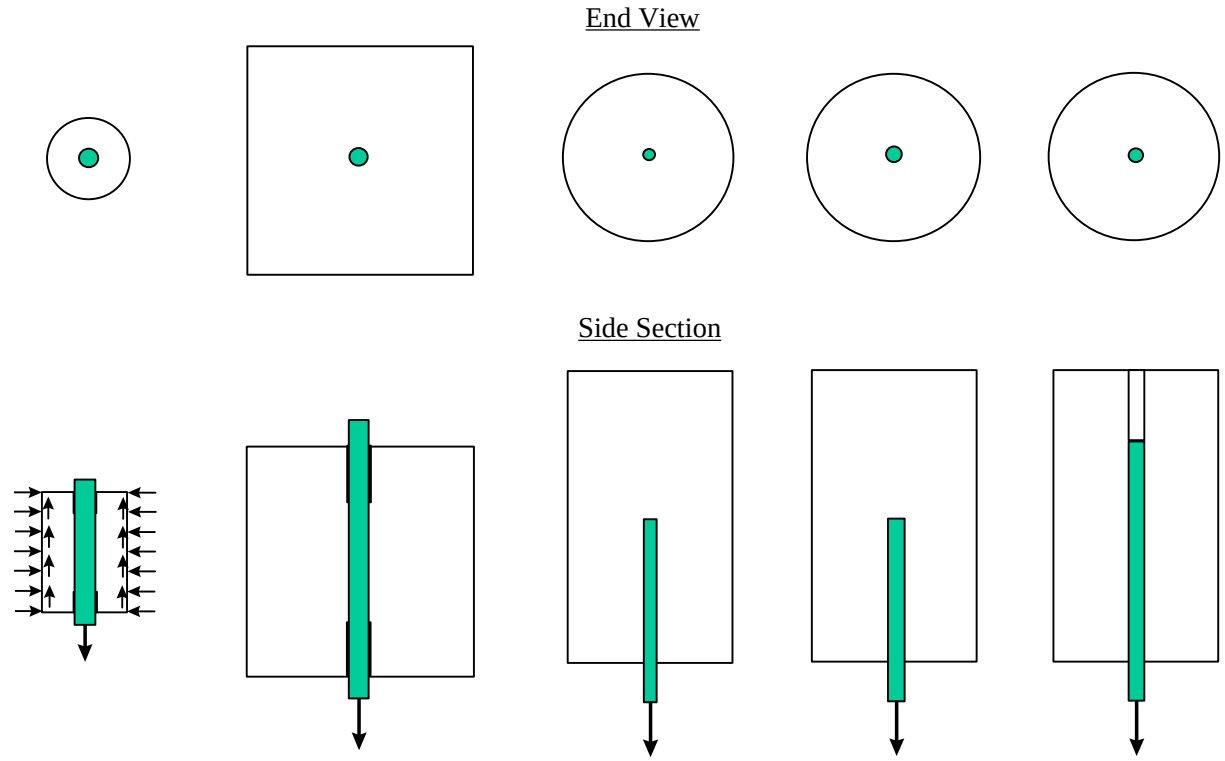


***Figure 7**. Schematics of the pull-out specimens.*

simulate the response of a given test requires a model of the bond specimen. The specimens were modeled using axisymmetric finite elements. Figure 8 shows the mesh for a model of the Malvar specimen. Since the actual specimen is pre-cracked, the axisymmetric model is idealized as having zero hoop stress.

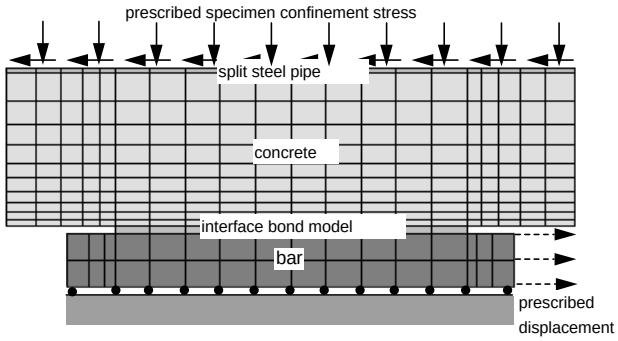


***Figure 8**. Bar-scale model of the Malvar specimen.*

For the validation specimens the concrete is idealized as an elastic solid under an axisymmetric stress and strain state with a pre-defined number of longitudinal cracks; these cracks are assumed to evolve concurrently and separate the concrete in the cracked region into equal size sectors. This axisymmetric idealization to incorporate the effects of longitudinal cracking originated with the analytical work of Tepfers (1979). The FE modeling approach used here follows the approach of Rots (1988), where the effects of longitudinal cracking are incorporated in an axisymmetric implementation of a "material model." Figure 9 represents the end-view of a specimen having three longitudinal cracks. Each crack is idealized as being planar with a process zone of infinitesimal thickness. The process zone in the plane of the crack represents the effects of crack bridging by the aggregates, has a finite length, and is commonly referred to as the *cohesive crack* (Hillerborg *et al.* [1976]) for this type of model. The behavior of the process zone is characterized by the following traction–crack opening relationship

$$s_{cr} = f_t(1.0 - \hat{w}^k) \tag{6}$$

where $\hat{w}$ is the ratio of the opening displacement of the cohesive crack and the critical crack opening (i.e., the minimum crack opening, $w_o$, for which there is no traction across the crack), $f_t$ is the tensile strength of the concrete, and $k$ is an model parameter. For the validation problems presented here, $k$ = 0.248 and $w_o$ is selected so that the model reproduces the estimated energy required to create additional crack surface (the so called *fracture energy*). This relationship is graphically depicted in Figure 10. When the tensile strength ($f_t$) of the concrete was not provided, it was estimated from the empirical relationship $f_t = 0.3\ f_c^{2/3}$ MPa, where $f_c$ is the compressive strength in MPa (see e.g., Eligehausen [1983] and CEB [1993]). The fracture energy of concrete specimen was estimated from the empirical relation suggested by CEB (1993): $G_F = G_{F0}(f_c/f_{c0})^{0.7}$, where $f_{c0}$=10 MPa and $G_{F0}$ is the base value of fracture energy that depends upon the maximum aggregate size.

For all of the specimens, the reinforcing bars were modeled as transversely isotropic. Based on estimates of the fiber volume fractions and mechanical properties of the fibers and matrix, the approximate formula of Hashin (1983) was used to estimate the transverse mechanical properties of the bars. Table 1 presents the material properties for the concrete and

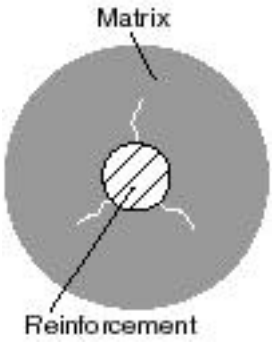


***Figure 9**. Longitudinal cracks in a section.*

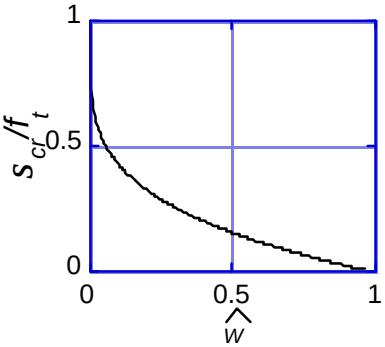


***Figure 10**. Traction-crack opening relationship.*

***Table 1: Material properties of FRP bars and concrete.***

| Material properties | Malvar (1994) | Tepfers et al. (1997) | Brown et al. (1993) | Larralde et al. (1993) | Larralde et al. (1994) |
|---|---|---|---|---|---|
| **FRP rebars:** | | | | | |
| **Young's moduli (GPa)** | | | | | |
| **Longitudinal $E_L$** | 39.8 | 42.9 | 51.7 | 51.7 | 51.7 |
| **Transverse $E_T$** | 9.29 | 10.9 | 14.3 | 14.3 | 14.3 |
| **Shear moduli (GPa)** | | | | | |
| **Longitudinal $G_L$** | 3.78 | 4.44 | 5.93 | 5.93 | 5.93 |
| **Transverse $G_T$** | 3.29 | 3.91 | 5.12 | 5.12 | 5.12 |
| **Poisson's ratios** | | | | | |
| **Longitudinal $n_L$** | 0.41 | 0.40 | 0.38 | 0.38 | 0.38 |
| **Transverse $n_T$** | 0.27 | 0.25 | 0.25 | 0.25 | 0.25 |
| **Concrete:** | | | | | |
| **Young's modulus (GPa)** | 30.7 | 29.1 | 30.7, 23.7, 20.0 | 28.7 | 30.7, 32.7, 32.3, 27.4, 28.8 |
| **Tensile strength (MPa)** | 2.79 | 2.0 | 2.28, 1.50, 0.90 | 1.89 | 2.28, 2.71, 2.62, 1.63, 1.92 |
| **Fracture energy (J/m$^2$)** | 0[1] | 64 | 70, 50, 32 | 80 | 92, 105, 102, 73, 81 |
| **Minimum crack opening (mm)** | 0[1] | 0.16 | 0.15, 0.17, 0.18 | 0.21 | 0.20, 0.19, 0.20, 0.22, 0.21 |

[1] pre-cracked concrete specimen

bar that were adopted in the analyses. The lists of concrete material properties for a given experimental study correspond to the sequence of tests shown in Table 2.

### 3.1 Calibration

Figure 11 shows the calibration results for the Malvar specimens at four different confinement stresses. The calibrated bond stress-slip responses are reproduced with acceptable accuracy. However, since only one test was performed at each confinement stress, the uncertainty in the experimental results has not been established. An important behavior that the model does reproduce is an increase in maximum bond stress and energy dissipation with increased confinement stress. The bond response of FRP and steel bars differ significantly in that the FRP bars exhibit a more ductile bond-stress slip behavior after the maximum bond stress is attained. The model is able to characterize this difference in behavior, but it does require a different calibration than was used for the steel bars. This relatively ductile bond behavior of FRP bars has been reported by several authors (see *e.g.*, Benmokrane *et al.* [1996], and Tepfers *et al.* [1997]). Malvar (1994) found that the surface structures of the FRP bars were significantly damaged, which suggests that the bond stress-slip behavior exhibited by these bars is strongly influenced by the progressive failure of the bar's surface structure.

The bond stress versus radial dilation results compare less favorably with the experimental data. Generally (for steel and FRP bars), the Malvar tests exhibit less radial dilation with increased confinement stress. This trend can be explained in terms of incremental work (Cox and Herrmann [1998]), but it is not consistently exhibited for this set of data. Nonetheless dilation is assumed to decrease with increased confinement stress in calibrating the flow rule which leads to significant differences in the predicted and measured radial dilations for confinement stresses of 500 and 2500 psi. These results suggest that for bars with this type of surface structure a relatively large variation in the radial response can be anticipated as compared with steel bars. The bond model predicts that the initial radial dilation will occur for much lower values of bond stress than observed in the experimental results. The experimental data is consistent with the behavior of dilatational materials – most of the dilation occurs near failure.

Even in the calibration experiments there are several possible sources of variation in the experimental results: (1) An increased variation in the radial dilation (relative to the results for steel bars) may be partially due to variations in the behavior of the FRP surface structure. (2) The pre-loading used by Malvar to pre-split the specimens produces an unknown amount of damage which may affect the bond response at different levels of confinement stress differently. (3) The radial dilations are small and may thus be difficult to measure accurately with the band apparatus. Variations in the experimental results can affect the interpretation of the calibration data. For example, the deviation of the radial dilation response from the expected trend implies that the longitudinal cracks may not be open in the actual experiment (for some states) as assumed, so the confinement stress at the bar may differ significantly from the value used in the model development. That is, if the longitudinal cracks are closed the external normal traction applied by the band apparatus is partially equilibrated by hoop stress in the concrete cylinder.

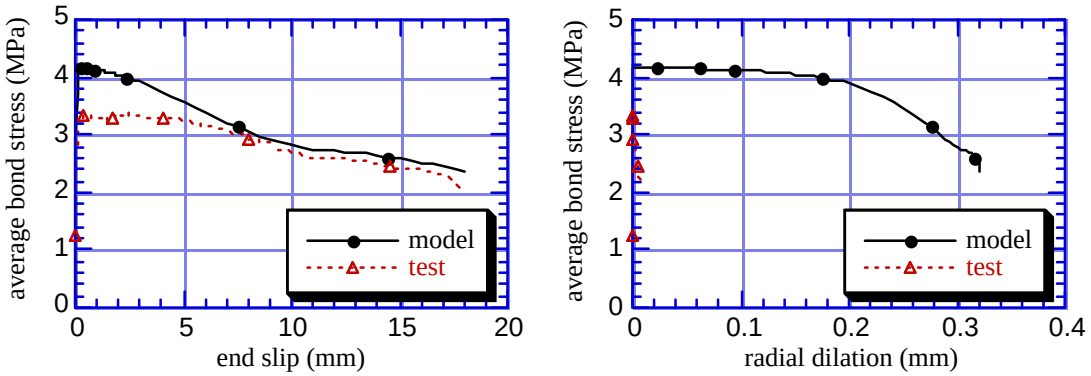


*(a) 500 psi (3.45 MPa) confinement stress*

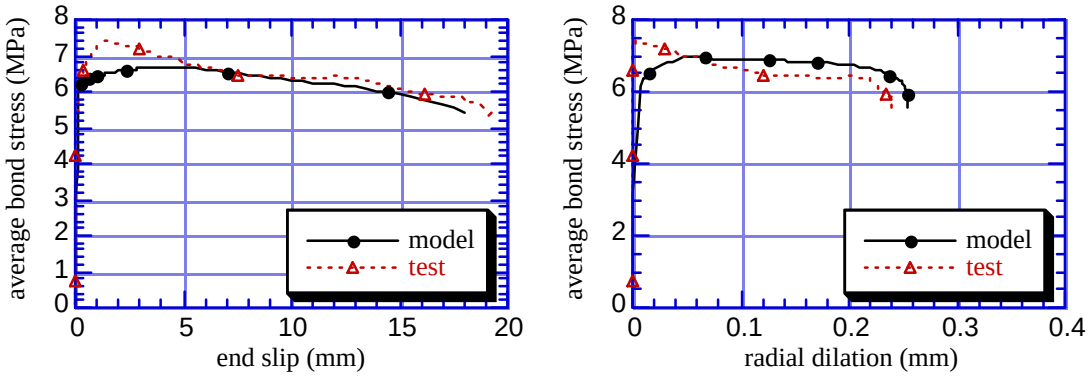


*(b) 1500 psi (10.3 MPa) confinement stress*

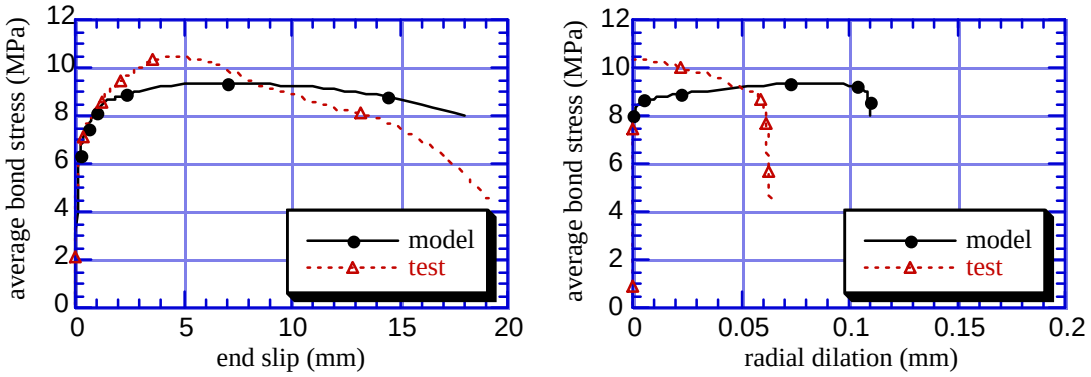


*(c) 2500 psi (17.2 MPa) confinement stress*

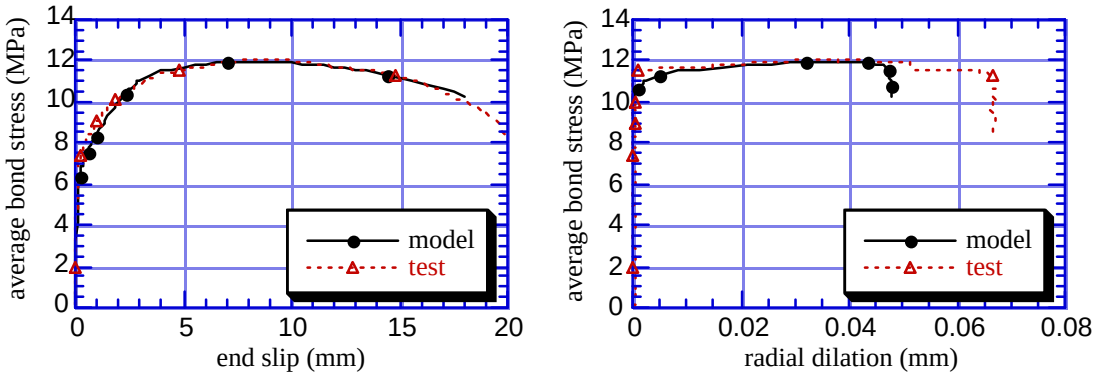


*(d) 3500 psi (24.1 MPa) confinement stress*

***Figure 11**. Calibration results for the Malvar "type d" specimen at 4 different confinement stresses.*

### 3.2 Validation

Tepfers *et al.* (1997) conducted several bond tests for FRP bars. Their specimens were cubic in shape and were cast within strong steel molds. Each specimen remained in a mold and thus was highly confined. They examined the bond behavior for various concrete strengths, bar diameters, and bond lengths. An axisymmetric model for the specimen was used in the numerical simulations; the diameter was chosen to be the width of the cube. Additional data for the models are given in Table 1. Data on the surface structure of the bar was not presented, so parameters such as indentation spacing were estimated from the photographs in their report.

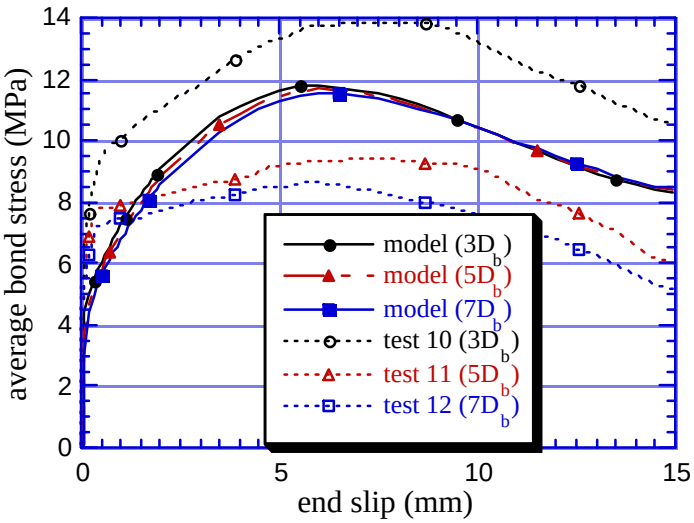


***Figure 12**. Test and numerical results of Tepfers et al. (1997) specimens.*

Figure 12 shows the comparison of the test and model results for specimens with three different embedment lengths ($3D_b$, $5D_b$, and $7D_b$).[JVC1] The difference between the model and experimental results may be significant, but it is difficult to make strong conclusions without a measure of experimental scatter. The model is not sensitive to the bond length, while the experiments appear to exhibit a strong inverse relationship between bond length and bond strength. However, these results must be considered in the context of other results obtained during the same experimental study. Many of the results did not show this trend, and the researchers concluded that "the ultimate bond stress is not influenced by the bond length in a clear way." The average bond strength obtained in the experiments differs with the average of the predicted values by about 9 percent, so if the differences are due to experimental scatter the model results are certainly acceptable as predictions of the mean responses.

Several approximations were made in the specimen model and in application of the bond model. Among the approximations were: (1) the axisymmetric model of the specimen and (2) estimates of the properties of reinforcing bars and concrete. As previously discussed, an underlying assumption in this work is that if the surface structure of the FRP bar and concrete strength are similar to the Malvar specimen, the elastoplastic bond model can be successfully applied to other specimens.

The last tests to be considered in the validation of the model are those by Brown and Bartholomew (1993), Larralde and Silva-Rodriguez (1993), and Larralde *et al.* (1994). The cylindrical specimens for these tests have the same dimensions, but the bars and concrete strengths differ. As previously noted, the surface structures appear to be similar to the "type d" bars of Malvar. For these tests the comparisons are limited to bond strength (Table 2). The bar diameters for some of these specimens are about half that of the calibration specimen, and two of the concrete strengths are very low. The model estimates most of the bond strengths with an accuracy comparable to the calibration results. Larralde and Silva-Rodriguez (1993) also reported the slip at failure. The model underestimated the slip values (*i.e.*, the model appeared to be stiffer than the experimental results); this inaccuracy is probably due to an aspect of the specimen behavior not captured with the current model. The specimens of Malvar and Tepfers *et al.* had an unbonded region of concrete at the loaded end of the specimen, while the specimens of these last two studies do not. Specimens not having an unbonded length can exhibit a more compliant behavior. The unusual predicted response of the F5-3 specimen (Larralde and Silva-Rodriguez [1993]) is a result of the interplay between the model's concurrent isotropic hardening

***Table 2: Test specimen data and results.***

| Experiments | Specimen Size ($D \times L$ or $L \times W \times H$) (mm) | Bar Diameter $D_b$ (mm) | Bond Length $L_b$ (mm) | Concrete Strength $f_c$ (MPa) | Maximum Bond Stress (MPa) | | |
|---|---|---|---|---|---|---|---|
| | | | | | Test | Model | "Error" |
| **Malvar (1994)** | 76×102 | 19 | 66.7 | 29.1 | | | |
| **500 psi** | | | | | 3.83 | 4.19 | 9 % |
| **1500 psi** | | | | | 7.40 | 6.68 | 10 % |
| **2500 psi** | | | | | 10.42 | 9.37 | 10 % |
| **3500 psi** | | | | | 12.07 | 11.95 | 1 % |
| **4500 psi** | | | | | 13.47 | 14.38 | 7 % |
| **Larralde *et al.* (1993)** | 152×305 | | | 23.8 | | | |
| **F3-3** | | 10.4 | 76.2 | | 9.12[1] | 8.97 | 2 % |
| **F3-6** | | 10.4 | 152.4 | | 8.53[1] | 8.28 | 3 % |
| **F5-3** | | 16.7 | 76.2 | | 6.35[1] | 5.81[3] | 9 % |
| **F5-6** | | 16.7 | 152.4 | | 5.61[2] | 5.51 | 2 % |
| **Larralde *et al.* (1994)** | 152×305 | | | | | | |
| **No. 1-3** | | 12.7 | 127.0 | 29.0 | 5.88[1] | 6.54 | 11 % |
| **No. 4-5** | | 12.7 | 127.0 | 35.2 | 7.33[2] | 7.69 | 5 % |
| **No. 7-9** | | 12.7 | 177.8 | 33.8 | 6.41[1] | 7.17 | 12 % |
| **No. 15** | | 12.7 | 228.6 | 20.7 | 5.61 | 4.90 | 13 % |
| **No. 22** | | 12.7 | 279.4 | 24.1 | 4.55 | 4.94 | 9 % |
| **Brown *et al.* (1993)** | 152×305 | 9.5 | | | | | |
| **Test-A** | | | 152.4 | 29.0 | 8.25 | 7.87 | 5 % |
| **Test-B** | | | 101.6 | 29.0 | 6.84 | 8.36 | 22 % |
| **Test-C** | | | 152.4 | 13.3 | 5.70 | 5.32 | 7 % |
| **Test-D** | | | 101.6 | 8.0 | 3.96 | 3.70 | 7 % |
| **Tepfers *et al.* (1997)** | 200×200 ×200 | 15 | | 25 | | | |
| **No. 10** | | | 45 | | 13.9 | 11.53 | 17 % |
| **No. 11** | | | 75 | | 9.5 | 11.40 | 20 % |
| **No. 12** | | | 105 | | 8.7 | 11.29 | 30 % |
| **average** | | | | | 10.7 | 11.41 | 7 % |

[1] average of 3 test results
[2] average of 2 test results
[3] This result corrsponds to the first peak in the predicted bond stress vs. end slip response. The model erroneously produced a second peak for this specimen that overestimated the bond strength by 43% at a large slip (~11.4 mm). This type of model response did not occur for any of the other tests.

and kinematic softening and can be improved by extending the range of kinematic softening; however, a more complete set of experimental data using a common set of FRP bars should be obtained prior to calibration refinements.

## 4. DISCUSSION AND CONCLUSIONS

The application of a bond model, which has been previously used to model bond between steel bars and concrete, has been extended to the application of bond for FRP bars. The model was developed to characterize the behavior resulting from the mechanical interaction between a slender reinforcing element that has a significant surface structure and the surrounding matrix. In previous studies a single calibration has been used to model the bond of "standard steel bars." However unlike steel bars, the surface structure of an FRP bar can be significantly damaged when large slips occur. The surface structure of FRP bars has not been tightly standardized, since many of the products are still evolving. Thus application of the phenomenological bond model to FRP bars will generally require recalibration for a particular bar, because the effects of many parameters (*e.g.*, geometry of the surface structure, and volume fraction and orientation of fibers in the surface structure) are difficult to quantify for this type of model.

The validation results presented here were for bond specimens that had bars with surface structures resembling those of the calibration specimen. The underlying assumption is that if the model is calibrated based upon a set of tests that address failure for a variety of stress states, the model can be used to predict the bond behavior of similar FRP bars; *i.e.*, the failure mechanisms will be similar to the calibration specimen, and their effects will be represented sufficiently accurately at the bar-scale. This modeling approach emphasizes characterizing the behavior that results from the mechanical interaction at a scale that is amenable to the analysis of structural components, but the model will not provide details on the dominant mechanisms of the bond failure nor on the state of damage of the FRP bar.

Most of the predicted bond strengths were within 15 percent of the measured values. This level of "accuracy" is better than anticipated considering the variation in the specimen properties, the surface structures of the FRP bars were not the same, the amount of experimental scatter is unknown, and there are several uncertainties in the specimen models. Additional studies are needed to quantify some of these uncertainties. In particular, an experimental study that considers several specimens (including the Malvar specimen for model calibration), provides data on experimental scatter, and uses a common bar (or set of bars) would allow a better evaluation of the proposed modeling approach. The assumptions associated with the specimen modeling also merit further investigation. Nonetheless, the preliminary results are encouraging and reflect the potential of using the model to characterize the behavior of concrete reinforced with FRP bars.

## 5. ACKNOWLEDGMENTS

This study was partially funded by a contract (N0024498P0366) from the Naval Facilities Engineering Service Center, Port Hueneme, CA.

## REFERENCES

ACI, Committees 408 and 440 (1994). "Summary papers for projects presented during the technical session on: Bond of fiber reinforced plastic (FRP) rebars and tendons," San Francisco, CA, March 21.

Alunno, R. V., D. Galeota, and M. M. Giammatteo (1995). "Local bond stress-slip relationships of glass fiber reinforced plastic bars embedded in concrete," *Materials and Structures*, vol 28, no. 180.

Benmokrane, B., B. Tighiouart, and O. Chaallal (1996). "Bond strength and load distribution of composite GFRP reinforcing bars in concrete," *ACI Materials Journal*, vol 93, no. 3, pp 246-253.

Belarbi, A., K. Chandrashekhara, and S. E. Watkins (1996). "Smart composite rebars with enhanced ductility," *Proceedings of the 11th ASCE Engineering Mechanics Specialty Conference*, May, pp 788-791.

Boothby, T.E., A. Nanni, C. . Bakis, and H. Huang (1995). "Bond of FRP Rods Embedded in Concrete," *Proceedings of the 10th ASCE Engineering Mechanics Specialty Conference*, May, pp 114-117.

Brown, V. L., and C. L. Bartholomew (1993). "FRP reinforcing bars in reinforced concrete members," *ACI Materials Journal*, vol 90, no. 1, pp 34-39.

CEB (1993). "CEB-FIP model code 90," Redwood Books, Trowbridge, Wiltshire, U.K.

Cosenza, E., G. Manfredi, and R. Realfonzo (1995). "Analytical modeling of bond between FRP reinforcing bars and concrete," *Non-metallic (FRP) Reinforcement for Concrete Structures*, L. Taerwe ed., pp 164-171.

Cosenza, E., G. Manfredi, and R. Realfonzo (1997). "Behavior and modeling of bond of FRP rebars to concrete," *Journal of Composites for Construction*, vol 1, no. 2, pp 40-51.

Cox, J.V. (1994). "Development of a plasticity bond model for reinforced concrete – Theory and validation for monotonic applications," *Technical Report: TR-2036-SHR*, Naval Facilities Engineering Service Center, Port Hueneme, CA.

Cox, J.V. (1996). "Elastic moduli of a bond model for reinforced concrete," *Proceedings of the 11th ASCE Engineering Mechanics Specialty Conference*, May, pp 84-87.

Cox, J. V., and L. R. Herrmann (1992). "Confinement stress dependent bond behavior, part II: A two degree of freedom plasticity model," *Proceedings of the International Conference on Bond in Concrete*, Riga, Latvia, CEB, vol 3, pp 11.11-11.20.

Cox, J.V., and L.R. Herrmann (1998). "Development of a plasticity bond model for steel reinforcement," *Mechanics of Cohesive-Frictional Materials*, vol 3, pp 155-180.

Cox, J.V., and H. Yu (1998). "A micromechanical analysis of the radial elastic response associated with slender reinforcing elements within a matrix," *Journal of Composite Materials*, submitted for publication.

Cox, J. V. and L. R. Herrmann. 1999. "Validation of a plasticity bond model for steel reinforcement," *Mechanics of Cohesive-Frictional Materials*, 4, to be published.

Ehsani, M. R., H. Saadatmanesh, and S. Tao (1997). "Bond behavior of deformed GFRP rebars," *Journal of Composite Materials*, vol 31, no. 14, pp 1413-1430.

Eligehausen, R., E. P. Popov, and V. V. Bertero (1983). "Local bond stress-slip relations of deformed bars under generalized excitations," *Report UCB/EERC-83/23*, University of California, Berkeley, CA.

Faoro, M. (1992). "Bearing and deformation behavior of structural components with reinforcements comprising resin glass fiber bars and conventional ribbed steel bars," *Proceedings of the International Conference on Bond in Concrete*, Riga, Latvia, CEB, vol 3, pp 8.17-8.26.

Faza, S. S., and H. V. S. GangaRao (1990). "Bending and bond behavior of concrete beams reinforced with plastic rebars," *Transportation and Research Record 1290*, pp 185-193.

Guo, J., and J. V. Cox (1998). "Modeling the mechanical interaction between FRP bars and concrete," *Proceedings of the 13th Annual Technical Conference on Composite Materials*, American Society for Composites, September, Baltimore, Maryland.

Hashin, Z. (1983). "Analysis of composite materials - A Survey," *Journal of Applied Mechanics*, vol 50, pp 481-505.

Hillerborg, A., M. Modéer, and P.A. Petersson (1976). "Analysis of crack formation and crack growth in concrete by means of fracture mechanics and finite elements," *Cement and Concrete Research*, vol 6, pp 773-782.

Larralde, J., and R. Silva-Rodriguez (1993). "Bond and slip of FRP rebars in concrete," *Journal of Materials in Civil Engineering*, vol 5, no. 1, pp 30-40.

Larralde, J., R. Silva-Rodriguez, J. Burdette, and B. Harris (1994). "Bond tests of fiberglass-reinforced plastic bars in concrete," *Journal of Testing and Evaluation*, vol 22, no. 4, pp 351-359.

Larralde, J., J. Mueller-Rochholz, T. Schneider, and J. Willmann (1998). "Bond strength of steel,

AFRP and GFRP bars in concrete," *The 2nd International Conference on Composites in Infrastructures*, H. Saadatmanesh and M. R. Ehsani ed., pp 92-101.

Malvar, L. J. (1994). "Bond stress-slip characteristics of FRP rebars," *Technical Report TR-2013-SHR*, Naval facilities Engineering Service Center.

Malvar, L. J. (1995). "Tensile and bond properties of GFRP reinforcing bars," *ACI Materials Journal*, vol 92, no. 3, pp 276-285.

Nanni, A., ed. (1993). *Fiber-Reinforced-Plastic (FRP) Reinforcement for Concrete Structures: Properties and applications*, Elsevier Science Publisher.

Rots J. G. (1988). "Computational modeling of concrete fracture," Dissertation, Dept. of Civil Engineering, Delft University of Technology, Delft, Netherlands.

Saadatmanesh, H., and M.R. Ehsani (1991). "Fiber composite bar for reinforced concrete construction," *Journal of Composite Materials*, vol 25, February, pp 188-203.

Schmeckpeper, E. R. and C.H. Goodspeed (1994). "Fiber-reinforced plastic grid for reinforced concrete construction," *Journal of Composite Materials*, vol 28, no. 14, pp 1288-1304.

Taerwe, L., ed. (1995), *Non-Metallic (FRP) Reinforcement for Concrete Structures, Proceedings of the 2nd International RILEM Symposium (FRPRCS-2)*, August, E&FN SPON.

Tepfers, R. (1979). "Cracking of concrete cover along anchored deformed reinforcing bars," *Magazine of Concrete Research*, vol 31, no. 106, pp 3-12.

Tepfers, R. (1998). "Bond between FRP-bars and concrete," *Technical Report Work No. 22*, Division of Building Technology, Chalmers University of Technology, Sweden.

Tepfers, R, G. Hedlund, and B. Rosinski (1997). "Pull-out and tensile reinforcement splice test with GFRP bars," *Technical Report Work No. 18*, Division of Building Technology, Chalmers University of Technology, Sweden.

Yonezawa, T., S. Ohno, T. Kakizawa, K. Inoue, T. Fukata, and R. Okamoto (1993). "A new three-dimensional FRP reinforcement," in *Fiber-Reinforced-Plastic (FRP) for Concrete Structures: Properties and Applications*, A. Nanni ed., Elsevier Science Publishers, pp 405-418.